Impact of SOA-Based Add-Drop Switch Nodes on High-Capacity Multicarrier Transmission for Metro-Access Networks

Impact of SOA-Based Add-Drop Switch Nodes on High-Capacity Multicarrier Transmission for Metro-Access Networks

Mariangela Rapisarda, Alberto Gatto, *Member, IEEE*, Paola Parolari, *Senior Member, IEEE*, Netsanet Tessema, Kristif Prifti, Nicola Calabretta, Christian Neumeyr, and Pierpaolo Boffi, *Senior Member, IEEE*

***Abstract*—Internet-generated traffic growth is forcing the development of new low-cost solutions in metropolitan area networks (MANs), in particular in the transceiver and network node architectures. Semiconductor optical amplifier (SOA)-based wavelength blockers can be used as fundamental building blocks to add and drop optical channels in the node architecture of several network hierarchical levels. Even if its employment is advantageous in terms of costs and amplification bandwidth, the SOA can operate in a nonlinear regime. This work analyzes the impact of SOA-based node crossing on high-capacity discrete multitone (DMT) signals. In order to properly evaluate the interplay between optical channels and SOA self-gain modulation, both external and direct modulations are considered. Dual-sideband (DSB) and single-sideband (SSB) DMT variants are taken into account, showing no significant difference in the impact of SOA crossing for external modulation of a DFB laser. On the other hand, an important effect of subcarrier suppression arises on DSB DMT direct modulation of a vertical cavity surface emitting laser (VCSEL), less consistent for SSB DMT direct modulation. The analysis allowed to properly choose the bias current for the SOA employed in an experimental setup used to evaluate the transmission performance in a MAN scenario including add-drop lossless switch nodes. The experimental results demonstrate that a target capacity of more than 50 Gb/s per channel can be achieved in a 116-km MAN network composed of an SOA-based metro-access node and two metro-core aggregators, considering the transmission of three 25-GHz spaced DMT channels.**

***Index Terms*—Discrete multitone modulation, metropolitan area networks, semiconductor optical amplifier.**

Manuscript received November 4, 2021; revised January 31, 2022; accepted March 21, 2022. Date of publication April 12, 2022; date of current version July 16, 2022. This work was supported in part by the European Union's Horizon 2020 research and innovation programme under Grant PASSION 780326, and in part by MICRAM, Opsys, and Tektronix. *(Corresponding author: Mariangela Rapisarda.)*

Mariangela Rapisarda, Alberto Gatto, Paola Parolari, and Pierpaolo Boffi are with the Dipartimento di Elettronica, Informazione e Bioingegneria, Politecnico di Milano, 20133 Milano, Italy (e-mail: mariangela.rapisarda@polimi.it; alberto.gatto@polimi.it; paola.parolari@polimi.it; pierpaolo.boffi@polimi.it).

Netsanet Tessema, Kristif Prifti, and Nicola Calabretta are with the Electrical Engineering Department Eindhoven, Technische Universiteit Eindhoven (TU/e), 5612 AZ Eindhoven, The Netherlands (e-mail: n.tessema@tue.nl; k.prifti@tue.nl; n.calabretta@tue.nl).

Christian Neumeyr is with Vertilas GmbH, D-85748 München, Germany (e-mail: neumeyr@vertilas.com).

Color versions of one or more figures in this article are available at https://doi.org/10.1109/JLT.2022.3164333.

Digital Object Identifier 10.1109/JLT.2022.3164333

I. Introduction

THE request of traffic produced by resource-hungry applications, such as 5G, ultra-high definition television, and mobile edge computing, is continuously increasing with a net positive market compound annual growth rate of 5%, expected up to 2022 [1]. This traffic is mainly concentrated close to where it is produced, so it involves small geographical areas in the proximity of the users: the adoption of new solutions to increase the offered capacity in access and metro networks is compelling. On the other side, the network elements have to provide flexibility to support agile traffic routing, scalability to cope with the variability of the traffic requirements, and sustainability in terms of costs and energy consumption. Moreover, traffic scaling forces "pay-as-you-grow" schemes to reduce capital and operating expenditures (CapEx-OpEx). In order to cope with these challenging requirements, a solution for future metropolitan area networks (MANs) envisages a modular approach in the design of the transmitter [2] and of the switching nodes [3]. In particular, sliceable bandwidth/bitrate variable transceivers (S-BVTs) [2] adopting directly-modulated (DM) vertical-cavity surface-emitting lasers (VCSELs) and arrays of coherent receivers can reduce footprint, costs, and energy consumption and allow to retrieve the received signal and compensate for the chromatic dispersion (CD) introduced at MAN distances (hundreds of kilometers). Moreover to achieve more adaptability to the channel and traffic conditions, multicarrier modulation formats, such as discrete multitone (DMT) [4] or orthogonal frequency-division multiplexing (OFDM), can be adopted. The bit- and power-loading at the digital signal processing (DSP) level, in fact, enables the manipulation of the transmission bandwidth to optimize the transmitted capacity and mitigate the spectrum fragmentation [5]. While OFDM requires high-bandwidth external IQ modulators, a DMT signal can be generated even by exploiting the direct modulation of the laser source. The use of dual-sideband (DSB) [6], [7] and single-sideband (SSB) [2] DMT signals to directly modulate C-band Indium phosphide (InP) VCSELs has already demonstrated high capacities for propagation distances around few tens of kilometers in a direct detection (DD) scheme [8]. The combination of VCSELs sources and DMT-based direct modulation assures the requested sustainability in terms of cost, power consumption,

and footprint for the future MAN. A transmitting module of 40 DM long-wavelength VCSELs covering the whole C-band has been designed and implemented, targeting 2 Tb/s capacity per photonic integrated circuit (PIC) [9], which corresponds to a target capacity per channel per polarization of 50 Gb/s. On the other side, MAN networks are designed in a layered topology [9] to comply with the traffic requirements, providing different functionalities at each hierarchical level (HL). So the node architecture at each HL has to comply with the different degrees of traffic aggregation; several technologies, such as InP monolithical integration or hybrid integration of low-loss Silicon photonics (SiPh) passives and InP actives, allow to deliver on-chip node functionalities [10]–[13]. The MAN node solution presented in [14] for the metro-access (MA) layers, proposes a simple architecture based on wavelength multiplexers/demultiplexers and arrays of semiconductor optical amplifier (SOA) switches. The obtained wavelength blocker (WBL) structure together with splitters/combiners is used to add and drop the optical channels and represents an attractive node solution, employing low-cost components and providing wideband amplification [15]. On the other side, SOAs can operate in the nonlinear regime, so, in order to be employed in future MAN networks based on the aforementioned S-BVT solution, it is important to evaluate the impact of SOA crossing on high-capacity DMT signals. This work performs a deep analysis on the effect of SOA gain compression due to self-gain modulation (SGM) on a single DSB and SSB DMT-modulated WDM channel generated by two differently modulated sources, an externally-modulated 1558-nm distributed feedback (DFB) laser and a 1535-nm DM-VCSEL, for several SOA saturation conditions. This analysis is preparatory to investigate the performance of a multichannel DMT transmission, measured in terms of transmitted capacity in a testbed including multi-span propagation taking into account the presence of a complete MA node, 25-GHz spaced traffic aggregators typical of metro-core (MC) nodes and up to 116-km standard single-mode fiber (SSMF) propagation [16].

The paper is organized as follows: Section II briefly describes the network node architecture at MA and MC levels. Section III discusses the impact of SOA crossing on a DMT signal generated by either external or direct modulation. Section IV characterizes the SOA impact in a multi-hop scenario and more than a hundred of kilometres of propagation. At last, the Conclusions summarize the main results.

II. Metro-Access and Metro-Core Node Architectures and Implementations

The MA nodes are low cost 2-degree reconfigurable optical add-drop multiplexer (ROADM) nodes based on WBLs for a simple add/drop functionality in the wavelength domain. The schematic representation of an MA node is shown in Fig. 1(b). At the input a de-multiplexing (DEMUX) arrayed waveguide grating (AWG) separates the wavelength channels. A 1:2 splitter is used to drop the signals to be sent to the lower network HLs; these signals are consequently blocked by the corresponding SOA gate switches. On the other hand, wavelengths to be forwarded to the next node cross the node by turning on the respective SOA gate switches. An access interface is necessary to control

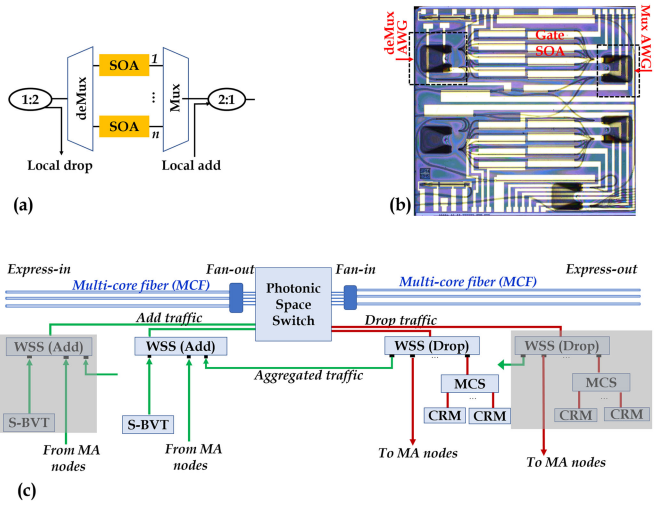

Fig. 1. Node architectures: (a) Schematic of the WBL-based MA node; b) Picture of the implemented InP PIC containing a WBL; c) MC switching node with components: photonic space switch, WSS, MCS, S-BVT, CRM.

the traffic from/to the lower HL nodes [17]. Fig. 1(b) shows an advantageous MA node architecture implemented by hybrid PICs containing a WBL, a 1:2 splitter and 2:1 combiner [17]; in this architecture the DEMUX and MUX AWGs pass/block 8 WDM channels. At the MC levels the node should handle the traffic both in the wavelength and in the space dimensions. The architecture of the MC node is shown in Fig. 1(c). The proposed MC node is thus a high capacity ROADM node which is equipped with color-less, direction-less, and contention-less (CDC) capability and can transparently switch space-division multiplexed (SDM) traffic via fan-out and fan-in in multi-core fibers (MCFs) or in fiber bundles (Fig. 1(c)). The photonic space switch, being the centre of the switching node, handles the traffic flow in the spatial domain in the express-in/out path. Wavelength selective switches (WSSs) and multi-cast switches (MCSs) are used in the add/drop paths to locally aggregate the traffic and to add/drop the traffic from the lower MA HLs, exploiting respectively S-BVTs and coherent receiver modules (CRMs) [18]. As the network grows, the new modules shaded in grey boxes in Fig. 1(c) are added in the drop and add directions to meet capacity demands with a modular approach. It is worth noticing that WBLs are key building blocks also for the WSSs and MCSs [18], thus it is of paramount importance to analyze the impact of WBL crossing on high-capacity signals travelling MA and MC nodes. In particular the WBL influence can be ascribed to the filtering action performed by the AWGs and to the SOA NL effects.

III. Analysis of SOA Impact on DMT Channels

In this Section we will focus on the effect of the crossing of a MA node, composed of two 100-GHz spacing AWGs and a SOA, on a high-capacity DMT signal; we will consider also the presence of a 25-GHz ROADM aggregator, typical of MC node architectures [19]. The analysis is performed on both externally- and directly-modulated sources, in order to highlight the impact of frequency chirp on SOA compression effect. The

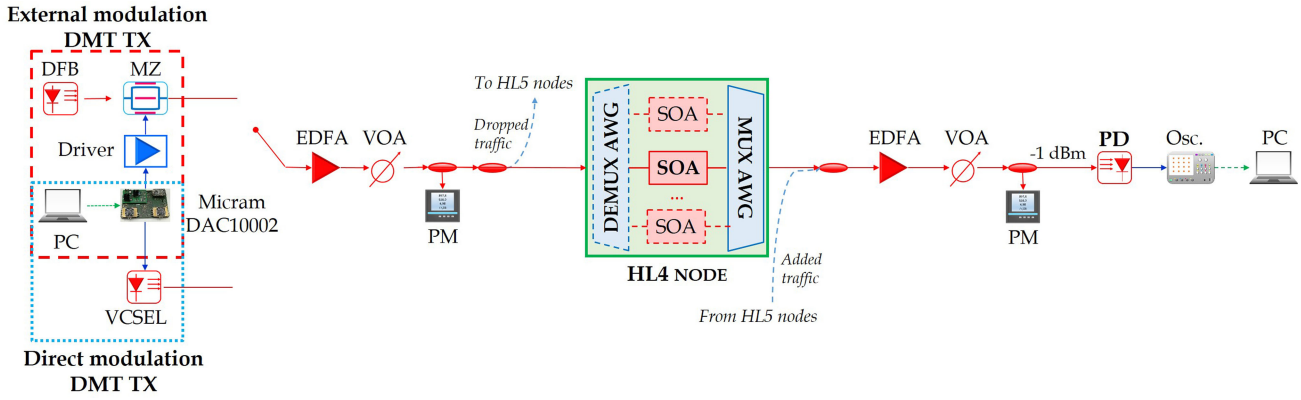

Fig. 2. Experimental setup for the evaluation of MA node crossing by DSB and SSB DMT-modulated optical signals.

performance is measured for several optical input powers and SOA bias currents to evidence the different behavior of the device, depending on its working conditions.

A. Experimental Setup

The performance evaluation is performed in terms of transmitted capacity variation and it is assessed by the experimental setup reported in Fig. 2 for both external and direct modulations. The externally-modulated source is composed of a 1558-nm DFB laser together with a 25-GHz intensity Mach-Zehnder (MZ) modulator, while the directly-modulated laser is a 1535-nm VCSEL with $\alpha = 3.7$ and $\kappa = 1.526 \cdot 10^{13}$ Hz/W chirp parameters. The directly-modulated VCSEL frequency response considers both the intrinsic modulation properties and the extrinsic device parasitic components [20], leading to an equivalent electrical modulation bandwidth of about 15 GHz. The modulating electrical DSB DMT signal is composed of 256 subcarriers in a 20-GHz range, so the subcarrier spacing is 78.125 MHz. A cyclic prefix (CP) of 2.1% of the symbol length is added. The DMT signal is generated by a 100 GS/s MICRAM DAC (DAC10002) with 40-GHz electrical bandwidth and 6-bit vertical resolution. In order to assess also the filtering effect of MC node crossing, a Finisar Waveshaper (WS4000s) is placed before the SOA to emulate the transfer function of a 25-GHz spacing WSS [19] to perform the optical filtering necessary to generate the SSB DMT signal, in both cases of external and direct modulation. The cascade of an Erbium-doped fiber amplifier (EDFA) and a variable optical attenuator (VOA) sets the input power to the MA node between -14 dBm and 0 dBm. The employed SOA is a 500-μm Optospeed 1550MRI/P device; Fig. 3 depicts the gain and the corresponding optical signal-to-noise ratio (OSNR) measured with 0.1-nm resolution for a continuous wave (CW) input signal for 100-mA and 225-mA bias currents. The bias current of the SOA ranging between these two values modifies the working conditions of the device in terms of OSNR and gain, having also a direct impact on saturation power and, therefore, on the SOA compression effect. In Fig. 3, in fact, it can be seen that the -1-dB (squares) and -3-dB (diamonds) gain compression points correspond to an input power of -14.2 and -9.2 dBm for the 225-mA bias current, whereas to -9 dBm and -2.5 dBm

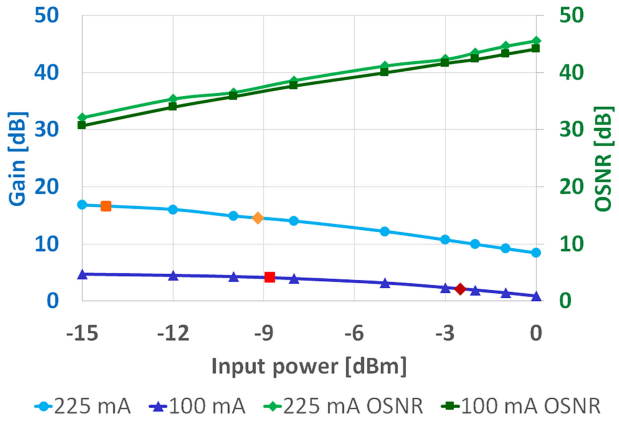

Fig. 3. Dependence of the CW gain G_{CW} and of the OSNR on the SOA input power for 100 mA and 225 mA bias currents. The squares and the diamonds indicate the -1-dB and -3-dB gain compressions respectively.

for the 100-mA one. Finally, the optical signal is received by a 14-GHz PIN photodiode keeping the received power to a fixed value of -1 dBm for all the measurement conditions; the received signal is then acquired by a Tektronix real-time oscilloscope with 8-bit vertical resolution, 100 GS/s and 33-GHz electrical bandwidth. Off-line processing provides digital symbol synchronization, CP removal, subcarriers phase recovery and demodulation, and bit error rate (BER) count. Optimal bit- and power-loadings (BL/PL) using Chow's algorithm [21] with a target BER of $4.6 \cdot 10^{-3}$ (in order to exploit an advanced hard-decision FEC code with 7% overhead [22]) are applied to adaptively assign the appropriate bit order at each subcarrier during the mapping procedure. The total transported capacity gives a measurement of the system performance for several SOA bias currents and SOA input optical powers. The SNR profiles obtained with uniform QPSK loading during the first step of the loading algorithm are used to underline the spectral dependence of the SOA presence at several saturation conditions.

B. Externally-Modulated Sources

Firstly, the impact of an SOA in strongly saturated conditions is analyzed for an externally-modulated source in case of a

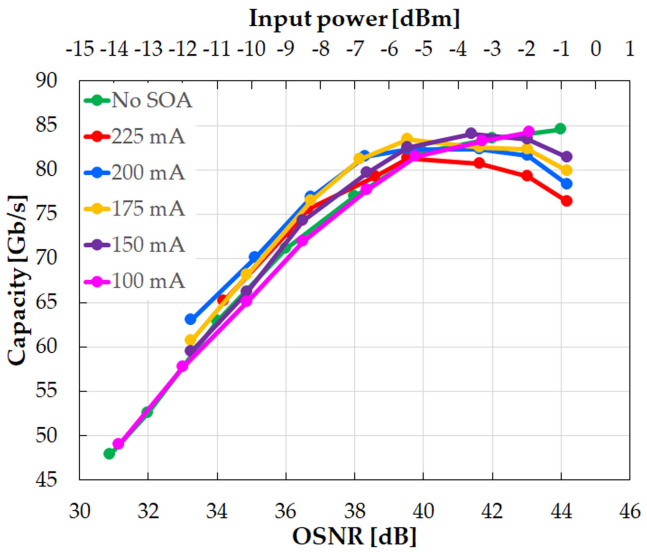

Fig. 4. Dependence of the capacity on the SOA input power and on the OSNR (0.1-nm resolution) measured at the receiver for DSB DMT external modulation. The secondary x-axis corresponds to the input power measured for a bias current of 175 mA.

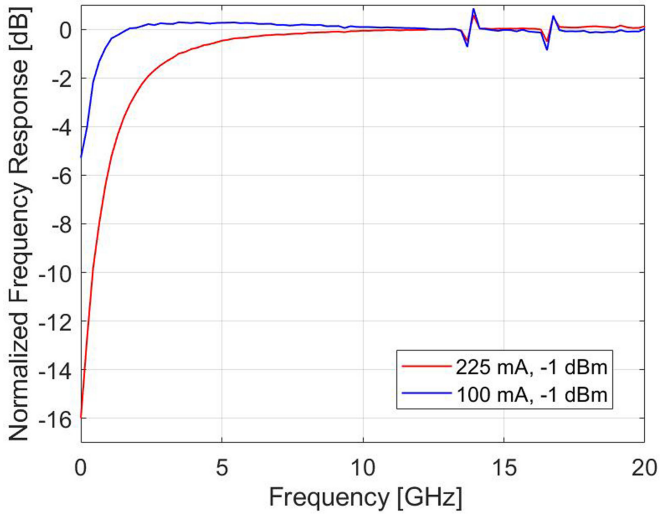

Fig. 5. SOA transfer function for bias currents of 100 mA and 225 mA and input power of −1 dBm.

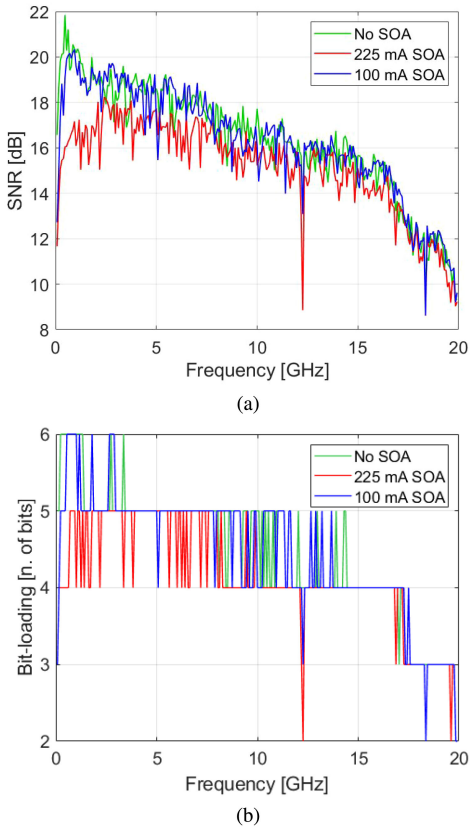

Fig. 6. (a) Measured SNRs and (b) bit loadings without SOA (green), for SOA bias current of 225 mA (red), and 100 mA (blue), and an input power of 0 dBm for external DMT modulation.

DSB DMT signal. Fig. 4 reports the capacity dependence on the SOA input power and on the OSNR (0.1 nm resolution) measured at the receiver for different SOA bias currents. As expected, the capacity increases for higher SOA input powers for each bias current in analysis, thanks to the higher OSNRs. However, the maximum capacity is obtained for OSNR around 40 dB, corresponding to an input power of −5 dBm and then slightly reduces at higher input powers, especially for higher bias currents. The capacity in these deeper saturation conditions is reduced by the more effective SOA gain compression, which, as described in [23], leads the SOA to act as an electrical high-pass filter. By analyzing the dependence of the capacity on the measured OSNR, we observe that for lower OSNRs the most significant contribution to the reduction of the capacity is the noise introduced by the SOA, in fact the capacities are comparable, no matter the SOA bias current. Actually at lower OSNRs, the green curve (without the SOA) is superimposed to the ones achieved with the SOA at the same OSNR. The equivalent electrical transfer function of the saturated SOA depends on the input and saturation optical powers, and by the carrier lifetime in the specific operational condition. Examples of the SOA transfer functions obtained in the small signal regime and measured by a vector network analyzer are shown in Fig. 5 for an input power of about -1 dBm at two different bias currents. Both the magnitude and the width of the low-frequency notch is significantly enhanced for higher bias currents, due to the strong saturation regime in which the SOA is operating, while the exploitation of a low bias current leads to a compression effect more limited in magnitude and width. The reported transfer functions influence the SNR of the different subcarriers composing the DMT signal, having an impact on the total capacity that can be achieved by the transmission system. Fig. 6(a) shows the SNRs obtained driving the MZM modulator with the DMT signal having all the 256 subcarriers loaded with QPSK modulation. By comparing the three curves it is evident that the SNR achievable by low-frequency subcarriers at 225 mA (red curve) is at least 3 dB lower than the corresponding values for 100 mA (blue curve), while for 100-mA bias current there is an almost perfect superposition with the case of SOA absence (green curve). Thus, when the SOA is working at lower bias

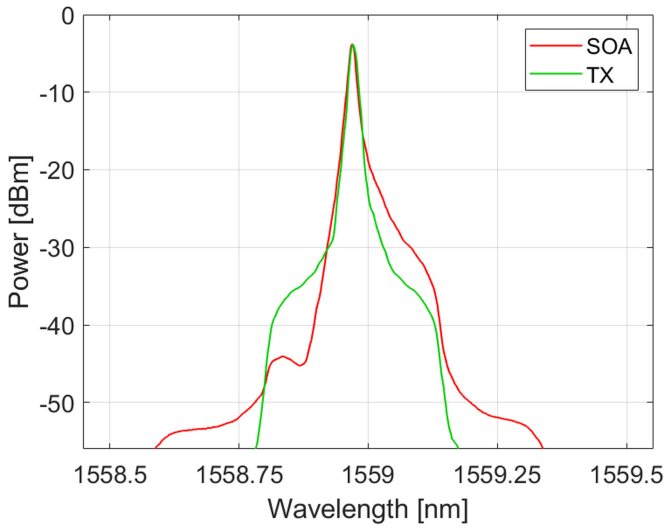

Fig. 7. Optical spectrum of the input signal (green) and at the output of the SOA (red) for an optical power of 0 dBm and a bias current of 225 mA, for DSB-DMT external modulation.

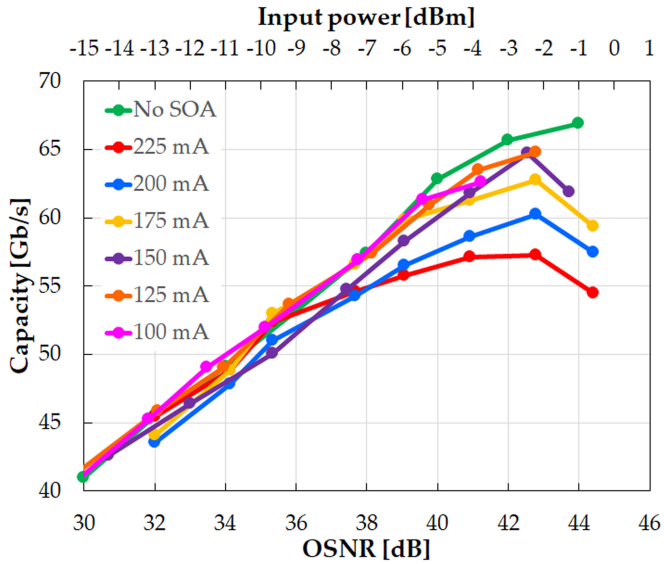

Fig. 8. Dependence of the capacity on the SOA input power and on the OSNR (0.1-nm resolution) measured at the receiver for SSB DMT external modulation. The secondary x-axis corresponds to the input power measured for a bias current of 175 mA.

currents, only slight distortions are introduced. This behaviour is reflected on the subcarrier modulation formats chosen by Chow's algorithm [21], as represented in Fig. 6(b): up to 4 GHz, the DMT subcarriers for the 225-mA bias current can be loaded just with 16- and 32-QAM, while both in absence of the SOA and with 100-mA bias current up to 64-QAM constellations can be transmitted.

Finally, increasing the optical input power leads to a vestigial-sideband (VSB) filtering effect [24] as shown in Fig. 7, where the optical spectra of the input signal (green) and of the amplified signal in highly-saturated SOA conditions (red) are displayed. During the amplification process of an intensity-modulated signal in an SOA, in fact, a frequency chirp $\Delta\nu_{SOA}(t)$ is superposed on the intensity-modulated (IM) signal, which can be expressed as

$$\Delta\nu_{SOA}(t) = -\frac{1}{2\pi}\cdot\frac{d\left[\phi_{SOA}(t)\right]}{dt}, \tag{1}$$

and further as [25]

$$\Delta\nu_{SOA}(t) = \Delta\nu_{in}(t) - \frac{\alpha_{SOA}\left(G_0-1\right)}{4\pi G_0}\cdot \cdot\frac{P_{out}(t)}{E_{sat}}\cdot\exp\left(-\frac{U_{in}(t)}{E_{sat}}\right), \tag{2}$$

where $\phi_{SOA}(t)$ is the phase acquired during signal amplification, α_{SOA} is the linewidth enhancement factor of the SOA, G_0 is the unsaturated gain, E_{sat} is the saturation energy, and $U_{in}(t)$ is the pulse energy in the leading part of the pulse. The optical signal at the SOA output is thus characterized by the presence of a negative chirp peak after the leading edge of the pulses and a positive chirp peak after the tailing edge of the pulses. This leads to the suppression of one sideband due to the power transfer from the higher frequency DMT sideband to the lower frequency one. For higher bias currents the conversion from optical DSB to optical VSB is emphasized due to a higher gain (so a higher output power) [24].

When we consider SSB externally-modulated DMT signals, achieved by means of the 25-GHz WSS optical filtering in the MC node, we obtain a similar behaviour in terms of transmitted capacity, as shown in Fig. 8. For OSNRs between 30 dB and 37 dB, the capacity increases with the OSNR, as it mainly depends on the noise introduced by the SOA, without the bias current influence. However, for SSB modulation, we reach a 50-Gb/s capacity for 33 dB OSNR while for DSB modulation the capacity is nearly 60 Gb/s: this is due to the impact of signal-signal beating interference (SSBI) [26]. For higher OSNRs, *i.e.*, higher input powers, the deeper saturation conditions induce the clamping of the obtained capacities especially for higher bias currents. The maximum rate capacity reduction is comparable with the one obtained with DSB DMT modulation, i.e., respectively around 15% for DSB and 14% for SSB DMT.

C. Directly-Modulated Sources

Novel MAN transmitters can take advantage of VCSEL direct modulation [27], thus it is worth performing the analysis for DMT-based directly-modulated sources. The direct modulation of a laser, in fact, generally introduces an additional phase term to the optical field. The phase term is the derivative of the instantaneous frequency variation $\Delta\nu(t)$, which is strictly related to the generated optical power by the relation

$$\Delta\nu(t) = \frac{\alpha}{4\pi}\left(\frac{1}{P(t)}\frac{\partial P(t)}{\partial t} + \kappa P(t)\right), \tag{3}$$

where α is the linewidth enhancement factor of the optical source, κ is a thermal coefficient depending on laser geometry, and $P(t)$ is the optical power emitted by the source. The presence of such frequency chirp leads to a spectral broadening and

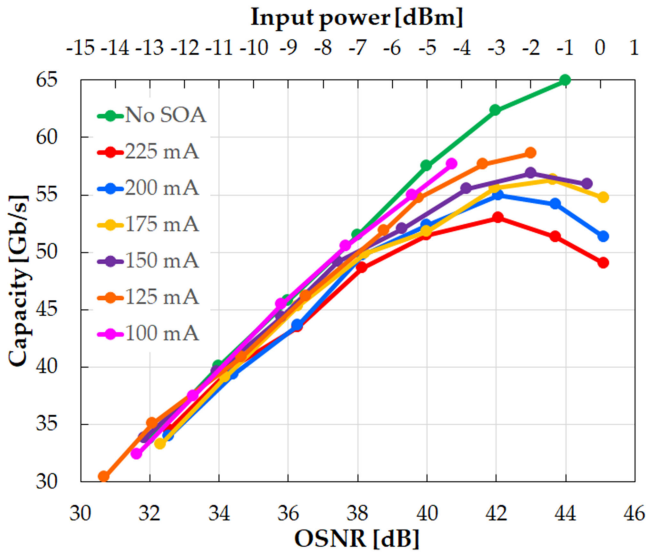

Fig. 9. Transmitted capacity for DM-VCSEL modulated with a 20-GHz DSB DMT signal in function of the SOA input power and on the OSNR (0.1-nm resolution) measured at the receiver. The secondary x-axis corresponds to the input power measured for a bias current of 175 mA.

to a detrimental interplay with the fiber chromatic dispersion; however, since the proposed MAN architecture is based on the exploitation of coherent detection, also after propagation in hundreds of SSMF kilometers the chirp interplay with CD can be neglected, thanks to the standard digital CD compensation processing. On the other hand, the spectral broadening is determined by the specific adiabatic and transient chirp parameters and by the modulation depth [28]. Since the chirp parameters are intrinsic properties of the source and no adjustment can be performed, to mitigate the impact of spectral broadening in case of tight filtering we optimized the modulation depth both for the DSB and SSB modulations, in order to achieve the best performance in terms of capacity. The optimization has been performed in absence of the SOA, leading to 11 mA and 8 mA modulation amplitudes in case of DSB and SSB modulations, respectively. The modulation depths have been maintained fixed for all the different SOA bias currents, in order to analyze the impact of SOA compression effect on chirp-impaired signals. Fig. 9 shows the dependence of the measured capacity on the SOA bias current and OSNR in case of DSB modulation. The capacity increases with the measured OSNR (*i.e.*, with the input optical power) till a given OSNR value of approximately 42 dB (corresponding to an input optical power around −3 dBm) for bias currents higher than 150 mA. When the power is further increased, the capacity decreases. The maximum rate capacity reduction of 22% is obtained at 225 mA. This percentage diminishes with the bias current, due to gain compression efficiency in different working conditions.

For input powers higher than −6 dBm (*i.e.*, OSNR values higher than 39 dB), the best performance of DSB DMT modulation is achieved for 125 mA, because it allows an adequate trade-off between gain compression and OSNR. For lower powers instead, the most impacting factor on the achievable transmitted capacity is the noise introduced by the amplifier, as visible in

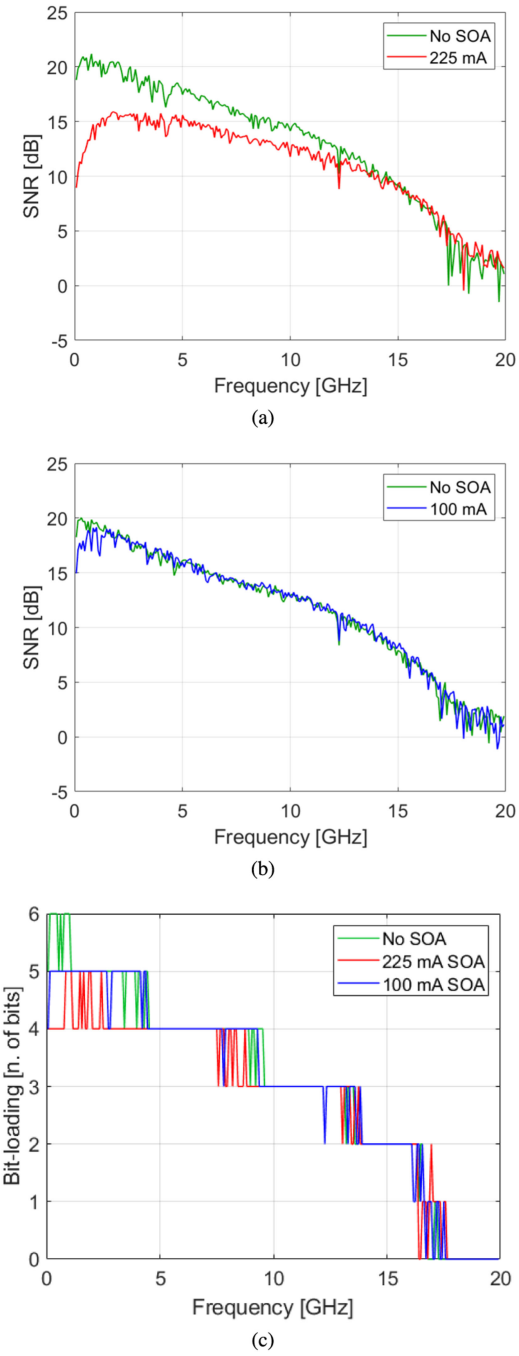

Fig. 10. Measured SNRs for 225-mA (a) and 100-mA (b) bias currents and −1 dBm input power along with the corresponding curves without the SOA (green curve) for DSB direct modulation. (c) Bit-loading without SOA (green), for a SOA bias current of 225 mA (red), and 100 mA (blue) at 40-dB OSNR measured at the receiver.

Fig. 9 where all the curves superimpose on the green one, i.e., without the SOA. The reference capacity of 50 Gb/s can be achieved for OSNRs higher than 38 dB, corresponding to input powers around −7 dBm, for all the bias currents except for 225 mA, which faces a not negligible gain compression even for lower powers.

Fig. 10 shows the impact of the SOA compression on the SNR obtained when loading all the DMT 256 subcarriers with

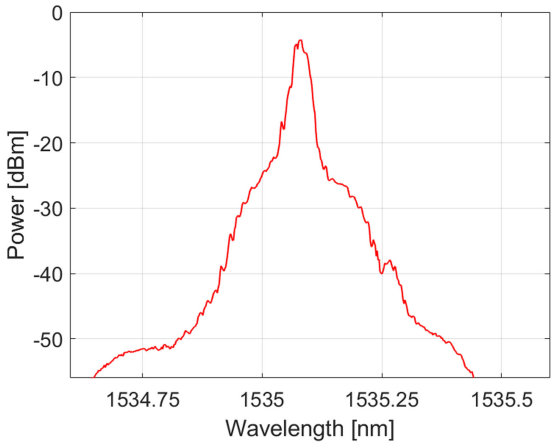

Fig. 11. Optical spectrum at the output of the SOA for an input power of 0 dBm and a bias current of 225 mA for the DM-VCSEL with a 20-GHz DSB DMT signal.

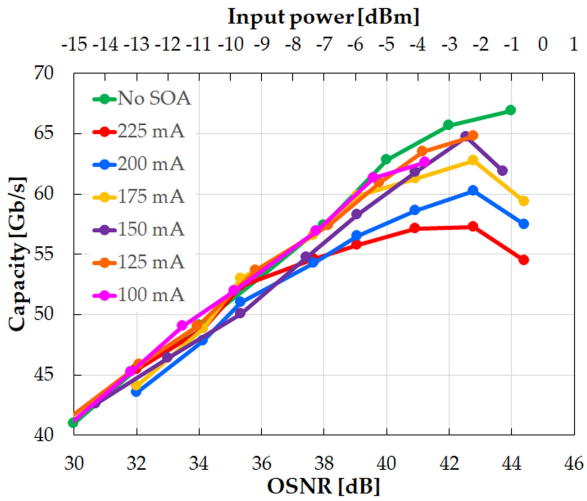

Fig. 12. Transmitted capacity for DM-VCSEL modulated with a 20-GHz SSB DMT signal in function of the SOA input power and on the OSNR (0.1-nm resolution) measured at the receiver. The secondary x-axis corresponds to the input power measured for a bias current of 175 mA.

QPSK modulation. In particular, the SNR behavior in presence of the SOA is compared with the reference SNR achieved without SOA amplification maintaining the same OSNR value, in order to fairly compare the performance of the DMT channel. Moreover, such comparison is performed at two different SOA bias currents (225 mA and 100 mA reported in Fig. 10(a) and (b), respectively) for −1 dBm input power, in order to highlight the effect of different gain compression regimes on the DMT frequency components. An evident frequency dip arises in the 225 mA condition, for which a reduction of about 10 dB appears in the low-frequency region. By comparing the green and red curves in Fig. 10(c), which display the actual DMT signal bit loading, it is evident that this SNR condition allows to load the first-GHz subcarriers just with a 16-QAM modulation instead of the 64-QAM one, transmitted in the SOA absence. The measured SNR is impaired by the SOA presence up to 13 GHz, from where no substantial difference with respect to the reference curve can be noticed and similar constellations can be thus used (Fig. 10(c)). The strong perturbation of the SNR profile in case of the high-bias regime causes the severe capacity reduction of more than 17 Gb/s with respect to the unamplified condition. On the other hand, in case of a lower bias current, no significant deviation from the reference SNR curve can be noticed. Only few subcarriers have to face a slight reduction, with a maximum drop of 3 dB for the first subcarriers, corresponding to the transmission of 32-QAM instead of 64-QAM constellations (Fig. 10(c)). Comparing the external modulation to directly-modulated sources, an evident decrease of the total supported capacity appears in the latter case. This reduction is mainly caused by the lower electro-optical bandwidth of the VCSEL source with respect to the external modulator one. Its effect is evident on the SNR curves, which in case of DM show values below 15 dB for subcarriers higher than 10 GHz, which limits the transmitted constellations to 8-QAM.

Fig. 11 shows the optical spectrum of the SOA output signal for a bias current of 225 mA and 0-dBm input power. Contrarily to what shown in Fig. 7, the DMT signal is still DSB. This phenomenon is due to the compensation of the SOA-induced chirp performed by the VCSEL chirp, which avoids the energy transfer between the sidebands.

Fig. 12 depicts the measurements performed in case of SSB optical filtering of the DMT directly modulated VCSEL, achieved by the MC node WSS, showing the dependence of the transmitted capacity on the measured OSNR. As for DSB-DMT signals, a peak in the transmitted capacity is reached for OSNRs around 42 dB. Again, from Fig. 12 it is evident that the capacity depends on the gain saturation for high input powers (*i.e.*, high OSNRs), while the predominant impairment for low bias currents is the ASE noise generated by the SOA. The curves for OSNRs up to 38 dB highlight that the measured capacity is comparable for every bias current, while for higher saturation conditions lower bias currents can achieve higher capacities, the OSNR level being the same. The maximum rate capacity reduction in case of SSB DMT modulation is 18%.

D. Discussion

A different effect of SOA crossing of signals generated with direct and external modulation (EM) is observed. Fig. 13 compares the normalized SNRs, *i.e.*, the curves obtained by subtracting the SNRs achieved without and with SOA amplification at equal bias current, input power and OSNR, for (a) DSB modulation and (b) SSB modulation with a bias current of 225 mA and 0-dBm input power. EM (blue curves) in presence of a highly-saturated SOA, shows a difference mainly in the SNR of subcarriers below 4 GHz for both DMT variants. On the other hand, with the VCSEL DM (red curves), the low-frequency dip is more pronounced for DSB modulation. As already stated, the main difference between EM and DM is related with the interplay between the chirp associated with DM and absent in case of EM and the SOA high-pass filtering. This is confirmed by the evaluation of the peak-to-peak signal amplitude at the SOA output, which is reduced of 0.77 dB for DM at equal input peak-to-peak signal amplitude.

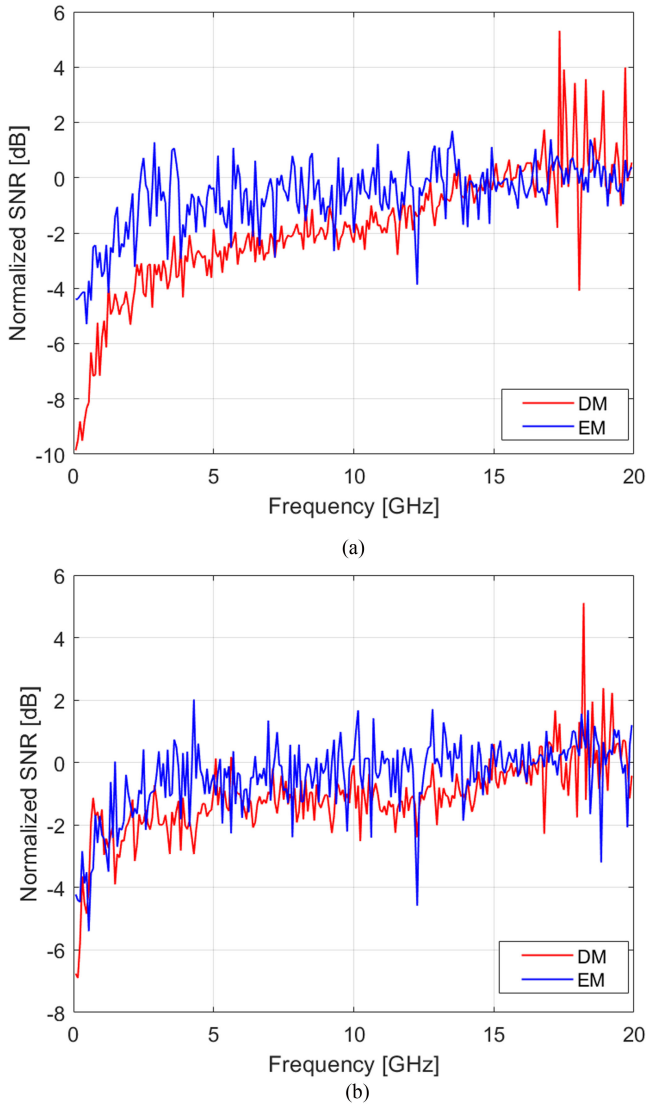

Fig. 13. Normalized SNRs for bias current of 225 mA and input power of 0 dBm for: (a) DSB modulation; (b) SSB modulation.

This behaviour reflects also on the obtained capacities which are higher with SSB DM than with DSB DMT DM. As already discussed, for high saturation conditions, SSB-DM DMT signals show up to 40% less SNR reduction in the low-frequency subcarrier range with respect to DSB modulation. At low input powers SSB DMT capacity is around 30% higher than the DSB-DMT one, and the target capacity of 50 Gb/s is reached for all the bias currents with SSB DMT between 34 dB and 35 dB OSNR with respect to the range 37-39 dB of DSB modulation. A reduction of only 8 Gb/s is faced when the OSNR is around 30 dB. When the normalized SNRs for DSB and SSB direct modulations are compared, the effect of SOA crossing is less detrimental in case of SSB modulation. SSB DM, in fact, is more robust to source frequency chirp [28] and it is also more resilient towards SGM, which is related with the carrier-to-signal power ratio (CSPR). The CSPR is defined as the ratio between the power of the CW carrier and the power of the modulated signal [26]:

$$CSPR = \frac{\overline{E_s}^2}{\sigma^2_{E_s}}, \tag{4}$$

where $\overline{E_s}$ indicates the mean of the modulated optical signal E_s and $\sigma^2_{E_s}$ is the signal variance, which essentially depends on its RF components. In fact, we measured a lower CSPR in case of SSB DM with respect to DSB DM, due to the partial filtering of the optical carrier along with an increase of the signal power, which compensates for the suppression of one sideband. Table I shows that at 225 mA and 0 dBm, the CSPR variation due to the SOA crossing is 1.5 dB higher in case of DSB DM with respect to SSB DM, as a result of a more significant impact of SOA SGM, which has a high-pass transfer function. When the saturation conditions are lower (*i.e.*, for lower bias currents and/or input powers) the CSPR values approach the ones obtained in absence of the SOA, and this confirms a reduced impact of the SOA SGM.

TABLE I
CSPR [IN dB] FOR DIFFERENT SOA OPERATING CONDITIONS ALONG WITH THE UNAMPLIFIED MEASUREMENT

Modulating signal	BTB	Input power	225 mA	125 mA
DM DSB DMT	16.91	0 dBm	20.67	18.44
		-14 dBm	17.61	17.23
DM SSB DMT	15.44	0 dBm	17.68	16.87
		-14 dBm	16.29	16.11

The study is useful to define the SOA operation conditions when exploited as WBL in MA and MC nodes. In particular the proper bias current has to be chosen to reduce the impact of the SOA in terms of signal distortion due to the high-pass filtering and of the output OSNR, as a trade off with respect to the provided gain which actually allows to compensate for PIC losses.

IV. MULTI-CHANNEL MULTI-HOP TRANSMISSION WITH A SOA-BASED MA-LIKE NODE

The analysis performed in the previous sections is helpful to choose the right bias current for the SOAs employed in an experimental setup used to evaluate the transmission performance in a MAN based on add-drop lossless switch nodes. In particular this section investigates the multi-hop, multi-channel transmission performance in presence of three DMT-based high-capacity channels: the multi-hop transmission includes a 100-GHz WBL MA node, two 25-GHz MC ROADM aggregators, and medium-reach propagation in SSMF. The experimental setup is shown in Fig. 14. A VCSEL emitting at 1535 nm is directly modulated with a DSB DMT signal composed of 256 subcarriers in 20-GHz bandwidth, with a CP of 2.1%. The presence of a MA ring (indicated with a dashed light-blue line) [29] is emulated by the cascade of a $L_2 = 9$ km SSMF span, the MA node, and another $L_3 = 6$ km SSMF span. The optical power reaching the SOA is -10.5 dBm, and, from previous section evaluations, a bias current of 200 mA was chosen to recover the losses in the MA link without introducing gain saturation impairments. The two other channels at 25-GHz spacing are added after the MA node, and aggregated with a programmable optical filter

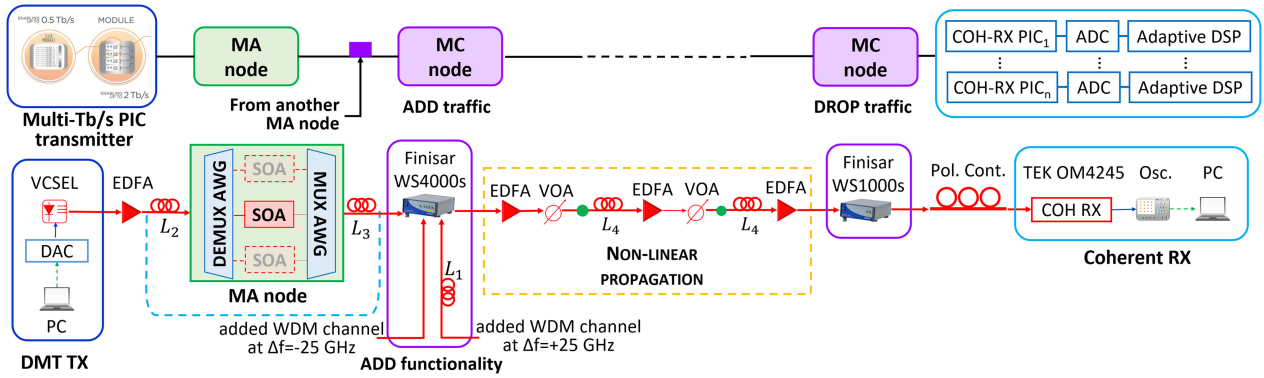

Fig. 14. Schematic of the network architecture with MA and MC node (top) along with the experimental setup (bottom).

(Waveshaper WS4000S) emulating the transfer function of a 25-GHz WSS [19], which performs the SSB filtering of all the channels as well. The channels propagate along two SSMF, $L_4 = 50$ km-long spans. At each span the per-channel launch power is set to 0 dBm. After the crossing of a programmable optical filter (Waveshaper WS1000S) emulating the transfer function of a DEMUX 25-GHz WSS [19], the signal is detected by a Tektronix OM4245 coherent receiver. Due to DM, the received signal is just intensity modulated and then a simplified adaptive off-line DSP can be used. The digital processing provides CD compensation, then the square moduli of the recovered I and Q components are performed and summed up to obtain the originally transmitted intensity signal. This approach avoids the use of phase and frequency recovery, reducing the complexity of the receiver DSP, but cancels the coherent detection advantages in terms of BER as a function of SNR with respect to DD [30]. Finally, the DSP performs the same functionalities described in Section III-A using a target BER of $4.6 \cdot 10^{-3}$; moreover the distortions due to nonlinear multichannel propagation are mitigated with a 3rd order Volterra equalizer [31].

In order to evaluate the effects of node filtering and of the SOA presence on DMT transmission, the capacities of a single channel in several conditions have been measured:

1) in BTB with the DEMUX WSS both with and without the 2 MA AWGs, without the SOA;
2) considering the entire MA ring, both with and without the SOA, with only the DEMUX WSS;
3) taking into account the whole MA ring, with both the add and the drop stages, *i.e.*, with both the 25-GHz WSS filters;
4) crossing the entire setup depicted in Fig. 14, with an overall propagation length of 116 km.

The multichannel propagation has been analyzed with the entire setup.

In Table II the measured capacities are summarized. The BTB DMT-DM SSB capacity with 25-GHz spectral occupancy is 68.3 Gb/s, which is taken as a reference. A capacity reduction of 4 Gb/s is faced when the two 100-GHz AWGs forming the MA node are crossed. The propagation along 16 km introduces a reduction of other 2 Gb/s with respect to the BTB case. The single-channel capacity is further reduced to 55.9 Gb/s in presence of the SOA, as it lowers the OSNR to 38 dB. The addition of the MC aggregation stage limits the capacity to

TABLE II
TRANSMITTED CAPACITIES WITH THE SETUP SHOWN IN FIG. 14

Distance	Configuration	Capacity
BTB	1 WSS (DEMUX)	68.3 Gb/s
	2 MA AWG, w/o SOA, 1 WSS	64.5 Gb/s
16 km	2 MA AWG, w/o SOA, 1 WSS	62.5 Gb/s
	MA node, 1 WSS	55.9 Gb/s
	MA node, 2 WSSs	54 Gb/s
116 km	Single channel	52.5 Gb/s
	3 25-GHz spaced channels	52.3 Gb/s

54 Gb/s due to the tight filtering performed by the cascade of two 25-GHz WSSs. In the single-channel case, in the emulated multi-hop configuration constituted of a MA ring, add and drop MC node stages, and an overall propagation in 116-km of SSMF, a capacity of 52.5 Gb/s can be reached. Thanks to DSP CD compensation the propagation in additional 100 km SSMF only slightly limits the capacity with respect to the 16-km propagation mainly due to an OSNR reduction. At last, a capacity of 52.3 Gb/s can be achieved in presence of three 25-GHz spaced channels. The 3rd order Volterra equalizer allows to control the NL impairments having only a reduction of 1.7 Gb/s with respect to 16-km single-channel propagation and to only 200 Mb/s with respect to 116-km single-channel propagation.

These measurements demonstrate that the VCSEL-based S-BVT approach previously introduced allows to achieve more than 50 Gb/s per channel even in presence of three 25-GHz spaced channels for propagation distances of more than 100 km, typical of MAN networks. However, it is important to properly choose the operation condition of the SOA, *i.e.*, its bias current, depending on the input power to the network nodes, in order to avoid distortions introduced by the SOA SGM. Moreover, the employment of a coherent receiver is mandatory for such propagation distances, so that the CD can be compensated and preferably nonlinear impairments can be mitigated with the implementation of equalization algorithms.

V. CONCLUSION

This paper has studied the impact of SOA-based MAN MA and MC network nodes on high-capacity DMT signals. The analysis has been performed for both external and direct DMT modulation in DSB and SSB variants to study the interplay

between DMT-modulated channels and SOA crossing. The SOA SGM causes the amplifier to behave as a high-pass filter, causing a distortion in the low-frequency subcarriers of the DMT signal. The analysis and the performed experiments evidenced that the presence of a SOA-based WBL has the greatest impact on the DSB DM-DMT signals. The laser chirp interplay with the SGM of the SOA in fact enhances the subcarrier suppression and, in case of DSB DMT DM, the SNR of the subcarriers is reduced for a wider spectral range and for a higher extent with respect to the external modulation. Even in presence of a deeply saturated SOA, DMT direct modulation of state of the art VCSELs guarantees that the target capacity of 50 Gb/s can be achieved for OSNR higher than 38 dB in case of DSB modulation, and higher than 34 dB for SSB modulation.

This preliminary analysis has allowed to investigate the impact of different SOA saturation conditions, depending on both the amplifier bias current and the optical input power, in order to properly set the operation conditions of the SOAs to be used in WBLs for low-cost MA and MC MAN nodes. The proposed solution has been validated in an experimental test-bed in a multi-hop, multi-channel, hundred-km MAN scenario. A target capacity of more than 50 Gb/s per channel has been demonstrated up to 116 km transmission by a DMT DM VCSEL based transmitter with three 25-GHz spaced channels crossing a MA SOA-based node and two MC add/ drop stages.

REFERENCES

[1] H. Adams, "Trends in metro optical networks," *IHS Markit Technol. Rep. Excerpts*, pp. 1–4, Mar. 2018.

[2] M. S. Moreolo *et al.*, "Modular SDN-enabled S-BVT adopting widely tunable MEMS VCSEL for flexible/elastic optical metro networks," in *Proc. Opt. Fiber Commun. Conf. Expo.*, 2018, pp. 1–3.

[3] N. Calabretta, K. Prifti, N. Tessema, X. Xue, B. Pan, and R. Stabile, "Photonic integrated WDM cross-connects for optical metro and data center networks," in *Proc. Metro Data Center Opt. Netw. Short-Reach Links II*, 2019, Art. no. 1094603.

[4] A. Gatto, M. Rapisarda, P. Parolari, and P. Boffi, "Discrete multitone modulation for short-reach mode division multiplexing transmission," *J. Lightw. Technol.*, vol. 37, no. 20, pp. 5185–5192, 2019.

[5] M. S. Moreolo *et al.*, "SDN-enabled sliceable BVT based on multicarrier technology for multiflow rate/distance and grid adaptation," *J. Lightw. Technol.*, vol. 34, no. 6, pp. 1516–1522, 2016.

[6] C. Xie *et al.*, "Single-VCSEL 100-Gb/s short-reach system using discrete multi-tone modulation and direct detection," in *Proc. Opt. Fiber Commun. Conf. Exhibit.*, 2015, pp. 1–3.

[7] A. Gatto, P. Parolari, C. Neumeyr, and P. Boffi, "Beyond 25 Gb/s directly-modulated widely tunable VCSEL for next generation access network," in *Proc. Opt. Fiber Commun. Conf. Expo.*, 2018, pp. 1–3.

[8] F. Karinou, N. Stojanovic, A. Daly, C. Neumeyr, and M. Ortsiefer, "1.55-m long-wavelength VCSEL-based optical interconnects for short-reach networks," *J. Lightw. Technol.*, vol. 34, no. 12, pp. 2897–2904, 2016.

[9] P. Boffi *et al.*, "Multi-Tb/s sustainable MAN scenario enabled by VCSEL-based innovative technological solutions," in *Proc. Metro Data Center Opt. Netw. Short-Reach Links III*, 2020, Art. no. 113080G.

[10] N. Andriolli, S. Faralli, X. J. M. Leijtens, J. Bolk, and G. Contestabile, "Monolithically integrated all-optical regenerator for constant envelope WDM signals," *J. Lightw. Technol.*, vol. 31, no. 2, pp. 322–327, 2013.

[11] K. Prifti, A. Gasser, N. Tessema, X. Xue, R. Stabile, and N. Calabretta, "System performance evaluation of a nanoseconds modular photonic integrated WDM WSS for optical data center networks," in *Proc. Opt. Fiber Commun. Conf. Exhibit.*, 2019, pp. 1–3.

[12] N. Tessema *et al.*, "SDN enabled dynamically re-configurable low-cost ROADM nodes for metro networks," in *Proc. 24th OptoElectron. Commun. Conf. Int. Conf. Photon. Switching Comput.*, 2019, pp. 1–3.

[13] N. Calabretta *et al.*, "Nanosecond wavelength and space optical crossconnect switches for high performance optical switches," in *Proc. 18th Int. Conf. Transp. Opt. Netw.*, 2016.

[14] R. Stabile, N. Tessema, K. Prifti, D. W. Feyisa, B. Shi, and N. Calabretta, "Photonic integrated nodes for next-generation metro optical networks," in *Proc. Metro Data Center Opt. Netw. Short-Reach Links IV*, 2021, pp. 55–60. [Online]. Available: https://doi.org/10.1117/12.2578846

[15] J. Renaudier *et al.*, "Recent advances in 100 nm ultra-wideband fiber-optic transmission systems using semiconductor optical amplifiers," *J. Lightw. Technol.*, vol. 38, no. 5, pp. 1071–1079, 2020.

[16] M. Rapisarda *et al.*, "Add-drop lossless switch node in multi-hop multi-Tb/s metropolitan area networks," in *Proc. Opt. Fiber Commun. Conf. Exhibit.*, 2021, pp. 1–3.

[17] K. Prifti, X. Xue, N. Tessema, R. Stabile, and N. Calabretta, "Lossless photonic integrated add-drop switch node for metro-access networks," *IEEE Photon. Technol. Lett.*, vol. 32, no. 7, pp. 387–390, Apr. 2020.

[18] N. Tessema *et al.*, "Modularly and hybrid integrated SiPh/InP wavelength blocker switch for metro networks," in *Proc. Eur. Conf. Opt. Commun.*, 2020, pp. 1–4.

[19] C. Pulikkaseril, L. A. Stewart, M. A. Roelens, G. W. Baxter, S. Poole, and S. Frisken, "Spectral modeling of channel band shapes in wavelength selective switches," *Opt. Exp.*, vol. 19, no. 9, pp. 8458–8470, 2011.

[20] S. Spiga, D. Schoke, A. Andrejew, G. Boehm, and M.-C. Amann, "Effect of cavity length, strain, and mesa capacitance on 1.5-m VCSELs performance," *J. Lightw. Technol.*, vol. 35, no. 15, pp. 3130–3141, 2017.

[21] P. S. Chow, J. M. Cioffi, and J. A. Bingham, "A practical discrete multitone transceiver loading algorithm for data transmission over spectrally shaped channels," *IEEE Trans. Commun.*, vol. 43, no. 2–4, pp. 773–775, Feb.-Apr. 1995.

[22] A. Alvarado, D. J. Ives, S. J. Savory, and P. Bayvel, "On the impact of optimal modulation and FEC overhead on future optical networks," *J. Lightw. Technol.*, vol. 34, no. 9, pp. 2339–2352, 2016.

[23] K. Sato and H. Toba, "Reduction of mode partition noise by using semiconductor optical amplifiers," *IEEE J. Sel. Topics Quantum Electron.*, vol. 7, no. 2, pp. 328–333, Mar./Apr. 2001.

[24] T. G. Silveira, A. L. Teixeira, A. P. Ferreira, and P. M. Monteiro, "All-optical vestigial sideband generation using a semiconductor optical amplifier," *IEEE Photon. Technol. Lett.*, vol. 18, no. 21, pp. 2212–2214, Nov. 2006.

[25] G. P. Agrawal and N. A. Olsson, "Self-phase modulation and spectral broadening of optical pulses in semiconductor laser amplifiers," *IEEE J. Quantum Electron.*, vol. 25, no. 11, pp. 2297–2306, Nov. 1989.

[26] D. Pilori, C. Fludger, and R. Gaudino, "Comparing DMT variants in medium-reach 100 G optically amplified systems," *J. Lightw. Technol.*, vol. 34, no. 14, pp. 3389–3399, 2016.

[27] P. Parolari, A. Gatto, C. Neumeyr, and P. Boffi, "Flexible transmitters based on directly modulated VCSELs for next-generation 50 G passive optical networks," *J. Opt. Commun. Netw.*, vol. 12, no. 10, pp. D78–D85, 2020.

[28] M. Rapisarda *et al.*, "Impact of chirp in high-capacity optical metro networks employing directly-modulated VCSELs," *Photonics*, vol. 5, no. 4, 2018, Art. no. 51.

[29] D. Larrabeiti *et al.*, "All-optical paths across multiple hierarchical levels in large metropolitan area networks," in *Proc. Asia Commun. Photon. Conf.*, 2019, pp. 1–3.

[30] P. Parolari *et al.*, "Preliminary assessment of photonic solutions based on C-band VCSELs for multi-Tb/s metro networks," in *Proc. 22nd Int. Conf. Transp. Opt. Netw.*, 2020, pp. 1–5.

[31] N.-P. Diamantopoulos, H. Nishi, W. Kobaya-shi, K. Takeda, T. Kakitsuka, and S. Matsuo, "On the complexity reduction of the second-order Volterra nonlinear equalizer for IM/DD systems," *J. Lightw. Technol.*, vol. 37, no. 4, pp. 1214–1224, 2019.